Transmembrane H⁺ fluxes and the regulation of neural induction in *Xenopus laevis*

Ho Chi Leung[1,*] [ORCID], Catherine Leclerc[2], Marc Moreau[2], Alan M. Shipley[3], Andrew L. Miller[1] [ORCID] and Sarah E. Webb[1] [ORCID]

[1]Division of Life Science and State Key Laboratory of Molecular Neuroscience, The Hong Kong University of Science and Technology, Hong Kong, China; [2]Centre de Biologie du Développement (CBD), Centre de Biologie Intégrative (CBI), Université de Toulouse, CNRS, UPS, F-31062, Toulouse, France and [3]Applicable Electronics, LLC, New Haven, CT, USA

Summary

It has previously been reported that in *ex vivo* planar explants prepared from *Xenopus laevis* embryos, the intracellular pH (pH_i) increases in cells of the dorsal ectoderm from stage 10.5 to 11.5 (i.e. 11–12.5 hpf). It was proposed that such increases (potentially due to H⁺ being extruded, sequestered, or buffered in some manner), play a role in regulating neural induction. Here, we used an extracellular ion-selective electrode to non-invasively measure H⁺ fluxes at eight locations around the equatorial circumference of intact *X. laevis* embryos between stages 9–12 (~7–13.25 hpf). We showed that at stages 9–11, there was a small H⁺ efflux recorded from all the measuring positions. At stage 12 there was a small, but significant, increase in the efflux of H⁺ from most locations, but the efflux from the dorsal side of the embryo was significantly greater than from the other positions. Embryos were also treated from stages 9–12 with bafilomycin A1, to block the activity of the ATP-driven H⁺ pump. By stage 22 (24 hpf), these embryos displayed retarded development, arresting before the end of gastrulation and therefore did not display the usual anterior and neural structures, which were observed in the solvent-control embryos. In addition, expression of the early neural gene, *Zic3*, was absent in treated embryos compared with the solvent controls. Together, our new *in vivo* data corroborated and extended the earlier explant-derived report describing changes in pH_i that were suggested to play a role during neural induction in *X. laevis* embryos.

Introduction

In cells, ion channels and transporters located in the plasma and organellar membranes generate ion-specific fluxes (reviewed by Meissner, 1983; Zhu *et al.*, 2010; Szabo and Zoratti, 2014; Xu *et al.*, 2015; Carraretto *et al.*, 2016). These generate electrical or chemical signals that play vital roles in specific biological events. The coordinated action of all the channels and transporters located in a membrane within a cell in so-called 'ion channel networks', results in the differential accumulation of ions (and therefore electric charge) across this membrane (Longden *et al.*, 2016). It is these distinct heterogeneities in charge across membranes that govern the overall electrical properties and therefore the signalling properties of a particular cell, tissue, organ or organism (Talevi and Dale, 1986; Gusovsky and Daly, 1988; De Simone *et al.*, 1998; Monteiro *et al.*, 2014; Luxardi *et al.*, 2015; Longden *et al.*, 2016).

It is well established that ion fluxes either into or out of cells are correlated with fertilization, development, differentiation, growth, regeneration, pattern formation and homeostatic regulation in a diverse array of biological systems, including animals, fungi and plants (Jaffe, 1979; De Simone *et al.*, 1998; Tosti, 2010; Tosti *et al.*, 2011; Hunter *et al.*, 2014; Tosti *et al.*, 2016; Carvacho *et al.*, 2018; McLaughlin and Levin, 2018). In addition to intracellular ion fluxes, developing organs and organisms often also require the activity of ions in the localized extracellular environment (Slack and Warner, 1973; Jaffe, 1979, 1981; Jaffe and Stern, 1979; Kline *et al.*, 1983; Nuccitelli, 1987; Rathore *et al.*, 1988; Altizer *et al.*, 2001). In plants, for example, one of the earliest reports demonstrated that an endogenous Ca²⁺ current was driven through the eggs of the brown fucoid algae *Pelvetia fastigiata* during zygotic polarization (Robinson and Jaffe, 1975). Soon after, an influx of K⁺ and an efflux of H⁺ were described in extending lily (*Lilium longiflorum*) pollen tubes (Weisenseel and Jaffe, 1976), and H⁺ currents were reported to traverse the growing roots and root hairs of barley (*Hordeum vulgare*; Weisenseel *et al.*, 1979). These early papers were quickly followed by a plethora of reports of ion fluxes entering and leaving a variety of tip-growing and polarizing plant structures from a wide range of different species (Miller *et al.*, 1986, 1988; Miller and Gow, 1989; Jones *et al.*, 1995; Kühtreiber and Jaffe, 1990; Feijó *et al.*, 1999; Messerli *et al.*, 1999; Zonia *et al.*, 2002; Xu *et al.*, 2006). With regards to fungi, early reports described ion currents traversing the growing hyphae of the water mould *Achlya bisexualis* (Kropf *et al.*, 1984) as well as the bread mould *Neurospora crassa* (McGillviray and Gow,

1987). More recently, transmembrane H^+ and Ca^{2+} fluxes have also been reported during apical growth and gravi-reception in stage 1 sporangiophores of the fungi *Phycomyces blakesleeanus* (Živanović, 2012).

In animals, Na^+ currents have been demonstrated in the near vicinity of regenerating limbs of the red-spotted newt *Notophthalmus viridescens* (Borgens *et al.*, 1977), as well as the regenerating tails of *Xenopus laevis* tadpoles (Tseng and Levin, 2008). Furthermore, transmembrane fluxes of H^+ and K^+ have been reported to play a role in the regulation of head and organ size during regeneration of the planaria *Schmidtea mediterranea* (Beane *et al.*, 2013); and an efflux of H^+ has been reported to occur during regeneration of the caudal fin in zebrafish (*Danio rerio*; Monteiro *et al.*, 2014). In addition, during embryogenesis, an early report demonstrated that the membrane of early *Xenopus* embryos is highly permeable to K^+ (Slack and Warner, 1973). Furthermore, effluxes of H^+, K^+, and HCO_3^- and influxes of K^+ and Ca^{2+} have been reported around the oocytes of the African clawed frog (*Xenopus laevis;* Moreau *et al.*, 1980; Faszewski and Kunkel, 2001). Ion fluxes have also been reported around the follicles and eggs of *Drosophila melanogaster* (Overall and Jaffe, 1985), an efflux of H^+ is reported to initiate the development of sea urchin (*Strongylocentrotus purpuratus*) eggs just after fertilization (Johnson and Epel, 1976), and more recently Ca^{2+} fluxes were found in the cleavage furrow of dividing zebrafish embryos (Chan *et al.*, 2015). An efflux of H^+ coupled to an influx of Ca^{2+} has also been reported to create favourable alkaline internal conditions for calcification events during shell formation of the freshwater common pond snail *Lymnaea stagnalis* (Ebanks *et al.*, 2010).

Ion currents are also associated with key physiological processes, such as those required for homeostatic regulation. For example, transepithelial ion fluxes have been recorded from H^+-pump rich cells located in zebrafish skin that help to regulate systemic acid–base homeostasis (Guh *et al.*, 2016), and Ca^{2+} fluxes have been reported exiting and entering the scales of zebrafish (Hung *et al.*, 2019) and sea trout (*Salmo trutta*; Jamieson *et al.*, 2021) as a short-term mechanism that helps in the regulation of the blood/interstitial fluid Ca^{2+} concentration during environmental and behavioural-induced calcemic challenges. In addition, ion fluxes have been reported to traverse a wide variety of neurons from a diverse range of species. For example, Ca^{2+} fluxes cross the cell membrane of the abdominal ganglion of the sea slug *Aplysia californica* when it is under oxidative stress (Duthie *et al.*, 1994). It has also been proposed that endogenous electrical currents might guide the rostral migration of neuroblasts in the brain of the neonatal mouse (*Mus musculus*; Cao *et al.*, 2013).

The flux of ions into and out of cells can be measured in the extracellular medium using a scanning ion-selective electrode technique (SIET). This is an ultrasensitive technique for measuring extracellular ion fluxes in a non-invasive manner via the use of a single ion-sensitive microelectrode (ISM), which is moved repeatedly between two measuring points located in close vicinity to the sample (Kühtreiber and Jaffe, 1990; Kochian *et al.*, 1992; Smith, 1995; Felle and Hepler, 1997; Hung *et al.*, 2019). Indeed, when the appropriate ion-selective ionophore sensor is loaded into the ISM tip, the detection of various ions at concentrations as low as at the picomolar level is possible with the SIET. For example, in recent years this technique has been used to detect small Ca^{2+} fluxes at the surface of excised metatarsal bones in the mouse (Marenzana *et al.*, 2005; Dedic *et al.*, 2018), and around the scales of adult zebrafish (Hung *et al.*, 2019) and sea trout (Jamieson *et al.*,

2021). It has also been used to measure effluxes of Na^+, Cl^-, K^+, Ca^{2+} and H^+ in wounds made in the skin of C57BL/6 mice (Sun *et al.*, 2015), and an efflux of H^+ in the excretory pore of *Caenorhabditis elegans* (Adlimoghaddam *et al.*, 2014). Prior to the development of the SIET, ion fluxes could still be identified using a simple voltage sensitive vibrating probe (Jaffe and Nuccitelli, 1974) in combination with an ion-substitution methodology (Reid *et al.*, 2007), where ions were selectively removed from the measuring medium and the effect on the current density recorded. Alternatively, intracellular Na^+ activity and pH could be measured continuously for several hours with sharp recessed-tip microelectrodes (prepared from Na^+-sensitive or pH-sensitive glass, respectively), which were inserted into cells (Thomas, 1972, 1974).

Here, we used the SIET to measure H^+ fluxes around *X. laevis* embryos between stage 9 to stage 12 (i.e. from ~7 hpf to 13.25 hpf), for the duration of gastrulation (Harland, 2000). Neural induction is initiated during blastula stage 8 and continues throughout the gastrula period (Baker *et al.*, 1999; Kuroda *et al.*, 2004), during which the ectodermal cells adopt either a neural or epidermal fate depending on their location with regards to the dorsal/ventral axis. The dorsal ectoderm is triggered to become neuroectoderm and, at the same time, the anterior–posterior axis is also initiated (Doniach *et al.*, 1992; Lamb and Harland, 1995; reviewed by Weinstein and Hemmati-Brivanlou, 1999; Harland, 2000). It has been reported that in *ex vivo* planar explants of *X. laevis,* the intracellular pH (pH_i) increases (indicating a decrease in intracellular $[H^+]$) specifically in the dorsal ectoderm cells from stage 10.5 to stage 11.5 (i.e. 11–12.5 hpf) and it was suggested that this change in pH_i plays a role in neural induction (Sater *et al.*, 1994). These experiments were conducted using the intracellular fluorescent pH indicator bis-carboxyethyl-carboxyfluorescein-dextran (BCECF-dextran), which was microinjected into 32-cell stage embryos, in conjunction with monitoring via emission ratio microfluorimetry. More recently, the SIET was used to measure distinct H^+ effluxes in *X. laevis* embryos from the two-cell stage to stage 6 (i.e. ~1.5 hpf to 3 hpf), and these were reported to play a role in left–right patterning (Adams *et al.*, 2006). However, these studies did not extend as far as neural induction. Therefore, it was of interest to confirm if distinct localized H^+ fluxes could be measured around *X. laevis* embryos at the onset of neural induction using this non-invasive method. In addition, vacuolar H^+-ATPases (V-ATPases) have been demonstrated to control the intracellular pH in many systems (Harvey, 1992). In *X. laevis* embryos, V-ATPase subunits have been shown to be localized asymmetrically as so-called 'fingers' extending from the vegetal cytoplasm into the animal hemisphere during the first few hours of development (Adams *et al.*, 2006). Therefore, we also investigated the activity of this ATP-driven H^+ pump on neural induction by treating embryos from stage 9 to stage 12 with the V-ATPase inhibitor bafilomycin A1 (Bowman *et al.*, 1988). The embryos were then fixed at stage 22 (i.e. 24 hpf) and the expression of the early neural gene, *Zic3* (Nakata *et al.*, 1997), was determined by *in situ* hybridization. The possible role of H^+ fluxes and the V-ATPase on neural induction in *X. laevis* is discussed.

Materials and methods

General *X. laevis* husbandry

Wild-type *X. laevis* were obtained from Nasco Agricultural Sciences (Fort Atkinson, WI, USA), and maintained in a

custom-made recirculating system in the Animal and Plant Care Facility at the HKUST. The system had a 5-µm water filter and ultraviolet (UV) light for disinfection. *X. laevis* were kept in 17 × 11.5 × 5.5-inch clear plastic tanks at a density of either two or three females or four or five males per tank in 12 L of frog water, which consisted of dechlorinated tap water containing 0.06 g L^{-1} Instant Ocean synthetic sea salt (Aquarium Systems, Inc., Mentor, OH, USA). They were maintained on a 12-h light/12-h dark cycle at ~18°C and with 70% humidity, and they were fed twice a week with ~1 g of Purina LabDiet® frog brittle (5LP3; Purina Mills, LLC, Gray Summit, MO, USA) per animal and once a week with blood worms (Hikari, Japan). All the procedures used in this study were performed in accordance with the guidelines and regulations set out by the Animal Ethics Committee of the HKUST and by the Department of Health, Hong Kong.

Embryo production

The procedure used to harvest the embryos was as described previously (Kay and Peng, 1991). Eggs were obtained from female *X. laevis* that had been primed between ~3 to 5 days prior to ovulation with 75 IU pregnant mare serum gonadotropin (Sigma-Aldrich Corp., St. Louis, MO, USA) to reinitiate oocyte meiosis. The females were then given a second injection of 500 IU human chorionic gonadotrophin (hCG; Sigma-Aldrich Corp.) at ~18–22 h prior to ovulation. The eggs were fertilized *in vitro* with macerated testis, and then dejellied with 0.1× Marc's Modified Ringer's solution (MMR: 100 mM NaCl, 2 mM KCl, 1 mM MgSO$_4$, 2 mM CaCl$_2$, 5 mM HEPES, pH 7.4) containing 2–3% L-cysteine hydrochloride (Sigma-Aldrich Corp.; pH 8.0) for ~3–5 min with gentle shaking. After dejellying, the embryos were rinsed five times with 0.1× MMR to remove the L-cysteine hydrochloride and then incubated in 0.1× MMR at 23°C until required. Staging was according to Nieuwkoop and Faber (1967).

SIET

Non-invasive measurements of real-time H^+ fluxes (pmol cm^{-2} s^{-1}) in the extracellular medium perpendicular to the surface of *X. laevis* embryos from stages 9–12 (i.e. from 7 hpf to 13.25 hpf) were accomplished using a SIET system (custom-designed and built by Applicable Electronics, LLC, New Haven, CT, USA) via an H^+ ISM. The technique is described in detail in Hung *et al.* (2019) in which we used a Ca^{2+} ISM, with the following modifications for measuring H^+ fluxes.

For the H^+ flux measurements, silanized glass microelectrodes were back filled with pH-buffered electrolyte (100 mM KCl and 50 mM HEPES, pH 7) to a column length of ~1 cm, and then front filled with Hydrogen Ionophore I Cocktail B (Sigma-Aldrich Corp.) to a column length of 25 µm. These glass microelectrodes were assembled and then connected to the microelectrode holder to form the ISM of the SIET system. ISMs were calibrated before every experiment to ensure their reliable performance during data collection (Fig. 1a). To achieve this, a three-point calibration was performed using three ion standard solutions. For H^+ flux measurements, 0.05 M Tris buffers at pH 6, pH 7 and pH 8 were used. A voltage value was taken for each ion standard solution and the Nernstian slope was calculated using the automated scanning electrode technique (ASET) software (Science Wares Inc., Falmouth, MA). The Nernstian slope was accepted at a theoretical value ± 4 (i.e. for H^+: 54.76–62.76), alternatively, the ISM was recalibrated or replaced (Kühtreiber and Jaffe, 1990). After calibration, the ISM

was also checked before each experiment to ensure that the background system noise was close to 0 pmol cm^{-2} s^{-1} (Fig. 1b). This background recording was performed using the experimental bathing medium (i.e. 0.1× MMR) in the scanning chamber minus an embryo.

Measurement of extracellular endogenous ionic currents

Before scanning via the SIET began, a dejellied stage 9 embryo was placed in the centre of the scanning chamber mounted in a groove made between two strips of silicon elastomer (Fig. 1ci). The scanning positions of the ISM were then set at a circumferential plane ~200 µm above the equator of the embryo using the computerized motion control system (Fig. 1cii–civ). In this way, the dorsal animal hemisphere could be scanned with the direction of ISM excursion being perpendicular to the surface of the embryo. An initial recording was acquired at a reference position ~5 mm away from the measurement positions. This allowed any background noise to be subtracted from the 'real' signals generated at the embryo surface. In addition to stage 9, scans were also performed around the embryos at stages 10, 11 and 12. The direction of excursion was different at each measurement point as it had to be perpendicular to the surface of the embryo (Fig. 1cii–civ). The calibration and background values (Fig. 1d, e) were checked once again after each experiment to verify that the ISM had functioned in a Nernstian manner throughout the data collection period. After scanning, the embryos were raised until they were at 3–4 days post-fertilization (dpf) to ensure that they developed normally (Fig. 1f). No measurements were made after stage 12 because, during the neural stages (stages 13–21), embryos undergo highly dynamic movements (Vandenberg *et al.*, 2011), due in part to the dramatic extension of the dorsal marginal zone (Keller, 1984). This prohibited close surface scanning due to potential damage to the delicate glass ISM.

Pharmacological treatment and *in situ* hybridization

The possible relationship between V-ATPase function and the development of neural structures was investigated by pharmacological means, using bafilomycin A1 (a V-ATPase antagonist; Bowman *et al.*, 1988). *In situ* hybridization was then conducted to detect the presence of the early neural gene, *Zic3*. The *in situ* hybridization method used was modified from Hemmati-Brivanlou *et al.* (1990). Linearized DNA fragments of pBluescript II KS-*Zic3* were prepared by digestion with the restriction enzyme, *Bam*H1, for 2–4 h at 37°C. To produce a *Zic3* DIG-labelled RNA probe, *in vitro* transcription was then performed using the linearized pBluescript II KS-*Zic3*, DIG RNA labelling mix and T3 RNA polymerase (11277073910 and 11031163001; Roche Diagnostics) following the manufacturer's instructions. The RNA pellets were then purified using phenol–chloroform extraction, as described in the manufacturer's instructions of the mMESSAGE mMACHINE® transcription kit, and then dissolved in 20 µl RNase-free water. The final concentration of RNA synthesized was measured using a NanoDrop 1000 spectrophotometer (Thermo Fisher Scientific).

Embryos were incubated with 0.1× MMR containing either 0.5 µM bafilomycin A1 and 0.4% DMSO (EMD Millipore; stock solution: 160 µM in DMSO) or 0.4% DMSO alone (control) from ~7 hpf to 13.25 hpf. At 13.25 hpf, the embryos were washed with 0.1× MMR for 3 × 5 min and then incubated in this same medium until they reached 24 hpf (i.e. equivalent to stage 22 in untreated, normally developing embryos). The bafilomycin
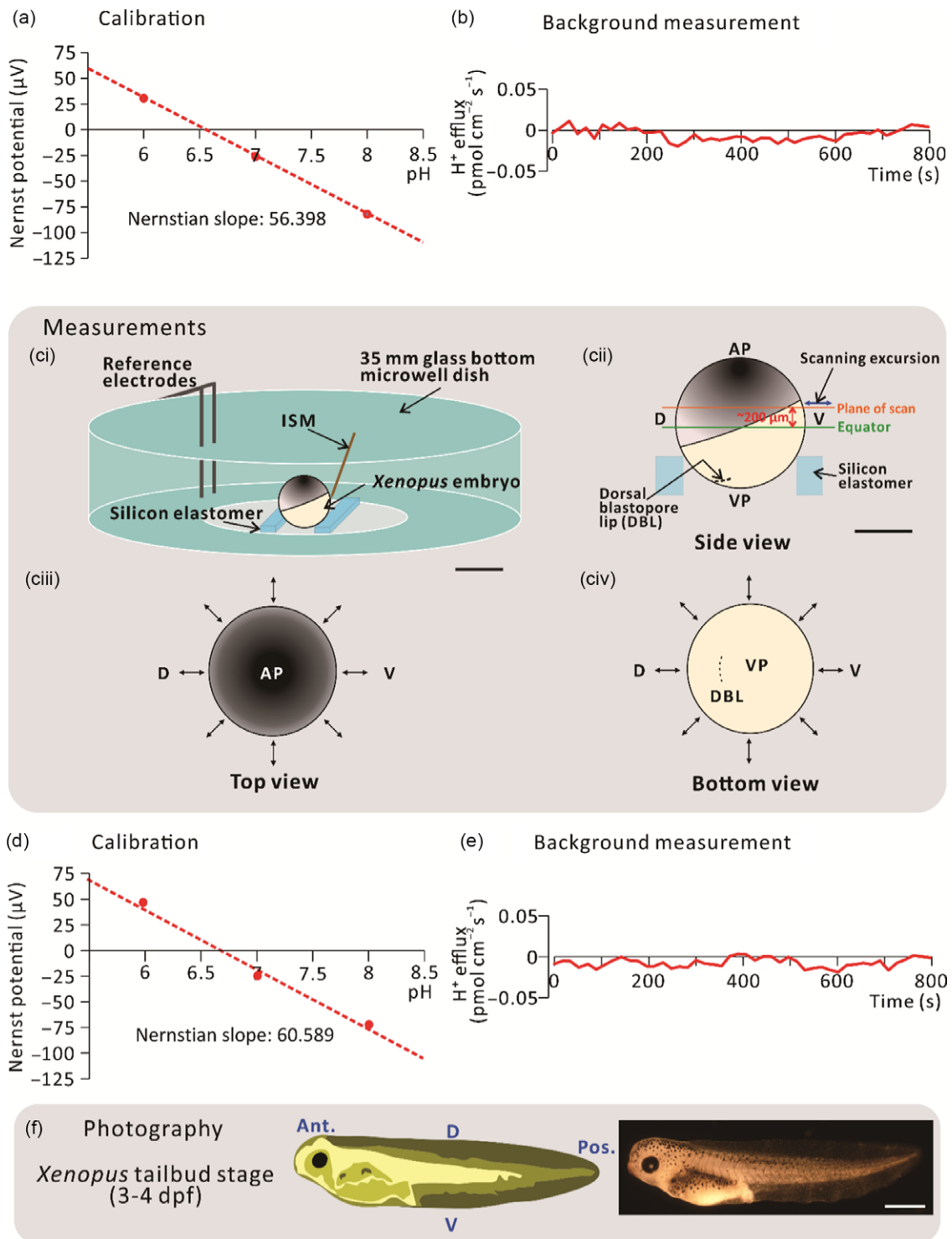
Figure 1. Schematic to show the SIET procedure. (a) An initial 3-point calibration was performed using three 'ion standard solutions', with a known concentration of H^{+}. In this case, calibration was performed at pH 6, 7 and 8. (b) An initial background recording was performed in the centre of a scanning chamber in the absence of an experimental embryo. (ci) Experiments were performed in a scanning chamber made of a 35-mm glass-bottomed microwell dish with pieces of silicon elastomer in the centre. (cii) Typically, the plane of scan was set at ~200 μm above the equator of the embryo. (ciii, civ) Images to show a representative sample scan around the embryo. Visualization at the (ciii) top and (civ) bottom of the embryo allows for precise positioning of the ion-selective microelectrode (ISM) close to the embryo surface. The ↔ symbol indicates the eight measuring positions around the circumference of embryos. (d) Recalibration and (e) background scans were also performed at the end of each experiment. (f) Scanned embryos were photographed at 3–4 dpf to ensure that they had developed normally. AP, VP, D, V, Ant., and Pos. are animal pole, vegetal pole, dorsal, ventral, anterior, and posterior, respectively. Scale bars, 1 mm (ci, f) and 500 μm (cii).

A1 + DMSO-treated or DMSO-treated embryos were fixed with MEMFA solution [0.1 M MOPS (pH 7.4), 2 mM EGTA, 1 mM $MgSO_4$ and 3.7% formaldehyde] at ~22°C for 1 h, and then washed with 2 mM $MgCl_2$ in PBS for 3 × 20 min. They were then dehydrated by sequential 5-min incubations through PBS containing increasing concentrations of methanol (i.e. 25%, 50%, 75% and

100%). The dehydrated embryos were stored for at least 1 week at −20°C, after which they were rehydrated by sequential 5-min incubations in PBS containing 0.1% Tween 20 (PBSTw) and decreasing concentrations (i.e. 100%, 75%, 50% and 25%) of methanol. The embryos were then permeabilized with proteinase K solution (10 μg proteinase K, 20 mM Tris (pH 7.6), 2 mM CaCl₂) for 7 min. Permeabilized embryos were washed with 0.1 M triethanolamine, pH 7.8 for 2 × 5 min, and then acetylated with 0.25% acetic anhydride in 0.1 M triethanolamine for 5 min. After subsequent rinsing with PBSTw, the embryos were fixed in PBSTw containing 3.7% formaldehyde for 20 min. They were then washed with PBSTw for 5 × 5 min, and then pre-hybridized with hybridization buffer [Hyb: 50% deionized formamide, 5× saline sodium citrate (SSC), 8.7 IU heparin, 1 mg Torula RNA, 1× Denhardt's solution, 0.1% Tween 20, 0.1% CHAPS, 50 mM EDTA] at 65°C for 4 h. The *Zic3* DIG-labelled RNA probe (at 1 μg ml⁻¹ in Hyb) was denatured at 80°C for 2 min before hybridization. Embryos were incubated with the denatured probe at 65°C overnight to allow time for it to hybridize with the endogenous target *Zic3* mRNA. Embryos were then washed with Hyb for 10 min and 2× SSC for 3 × 20 min at 65°C. Non-hybridized RNA was then digested with 2 μg ml⁻¹ RNase A in 2× SSC at 37°C for 30 min, after which embryos were washed with 2× SSC for 10 min at room temperature and 0.2× SSC at 65°C for 2 × 30 min. The embryos were then blocked with Blocking Reagent (2 g; 11096176001; Roche Diagnostics) in 1× maleic acid buffer (MAB) at room temperature for 1 h, after which they were incubated at room temperature with Blocking Reagent containing alkaline phosphatase-tagged anti-digoxigenin (11093274910; Roche Diagnostics), at a dilution of 1:4000 for 4 h. Embryos were then washed with 1× MAB overnight, after which they were stained with BM-Purple (11442074001; Roche Diagnostics) for ~4 h until purple staining was observed. The embryos were then fixed in Fixative B (1× SSC containing 10% acetic acid and 9.25% formaldehyde) for 1 h and depigmented in bleach solution (1× SSC containing 5% formamide and 10% H₂O₂) for 2 h. After rinsing with 1× SSC, images were acquired using a Nikon AZ100 Multizoom microscope system.

Top-illuminated stereomicroscopy

To study the morphology of embryos and the localization of mRNA after *in situ* hybridization, top-illuminated microscopic images were obtained using an AZ100 Multizoom microscope system with a DS-5Mc Colour Digital Camera Head in conjunction with the Digital Sight DS-U2 microscope camera controller and ACT-1 Version 2.63 software (Nikon Instruments, Inc., Tokyo, Japan). Top illumination was provided by a Schott KL 1500 electronic light source (Schott AG, Mainz, Germany). For live imaging, embryos were anaesthetised with 0.1× MMR containing 0.2 g L⁻¹ MS-222 just prior to imaging.

Statistical and computational analysis

IBM SPSS Statistics 23 (IBM, Armonk, NY, USA), Microsoft Office Professional Plus Excel 2013 (Microsoft Corp., Redmond, WA, USA), and CorelDRAW X8 (Corel Corp., Ottawa, ON, USA) were used for statistical analysis, graph plotting and figure preparation, respectively. Two-way analysis of variance (ANOVA) and post hoc Tukey's honest significant difference tests were performed to analyze the significance of the data.

Results

Identification of endogenous H⁺ currents using the SIET

We conducted extracellular non-invasive SIET measurements around embryos between stages 9–12 (i.e. from ~7–13.25 hpf) using an H⁺-specific ISM (Fig. 1). At each developmental stage, the H⁺ flux measurement made at a reference position ~5 mm from the embryo surface was ~0 pmol cm⁻² s⁻¹. In contrast, the minimum H⁺ efflux measured around the embryos was ~0.1 pmol cm⁻² s⁻¹ (Fig. 2). At stage 9 (Fig. 2a), a near-constant H⁺ efflux of ~0.1 pmol cm⁻² s⁻¹ was maintained at all the measuring locations around the embryos. At stage 10 (Fig. 2b), the H⁺ effluxes from the left (L), left dorsal (LD), dorsal (D) and right dorsal (RD) locations appeared to be slightly higher than from the other regions, but no significant differences were found between all the measurement locations around the embryos. At stage 11, the H⁺ efflux from the dorsal region (especially in positions LD and D) was elevated, showing values of ~0.2 pmol cm⁻² s⁻¹, which were significantly higher than the effluxes of ~0.1 pmol cm⁻² s⁻¹ detected on the left ventral (LV) side (Fig. 2c). At stage 12, a distinct H⁺ efflux of ~0.55 pmol cm⁻² s⁻¹ was detected on the dorsal (D) side of embryos (Fig. 2d). This was significantly higher than the effluxes detected at all the other measurement positions. These same data are also presented on a radial column chart (Fig. 3), which clearly shows that there was an increase in H⁺ efflux from stage 9 to stage 12 in all the measurement locations, with a more prominent H⁺ efflux generated on the dorsal side of embryos. In addition, at stage 12 (i.e. the end of gastrulation), the H⁺ effluxes in the dorsal (D) and RD locations were significantly greater than those measured in the same locations between stages 9–11.

Effect of bafilomycin A1 on the gross morphology and expression of Zic3 in embryos at 24 hpf

Following the discovery of a distinct H⁺ efflux at the dorsal animal hemisphere of embryos between stages 11 and 12, we investigated whether H⁺ signalling might play a role in neural induction. We treated embryos with bafilomycin A1 to block the activity of this ATP-driven H⁺ pump from stages 9–12, and then investigated the effect of this inhibition on the gross morphology of embryos, as well as the expression of the early neural gene *Zic3* at 24 hpf. As the stock solution of bafilomycin A1 was prepared in DMSO, some embryos were treated with the same concentration of DMSO alone as controls. In the DMSO-treated control embryos, unfused and fused regions of the neural fold, as well as the cement gland and eye anlagen were all clearly visible at 24 hpf (i.e. stage 22; Fig. 4ai, 4aii, see white, blue, yellow, and black arrowheads, respectively), therefore suggesting normal development. In contrast, embryos treated with bafilomycin A1 (Fig. 4bi, 4bii), did not complete gastrulation, as shown by the obvious yolk plug at the vegetal pole (pink arrowheads). The DMSO- and bafilomycin A1-treated embryos were fixed at 24 hpf and then *in situ* hybridization was conducted to visualize the expression of *Zic3*. In the DMSO-treated embryos, *Zic3* was expressed in the telencephalon, diencephalon, mesencephalon and rhombencephalon (Fig. 4c), as first described by Nakata *et al.* (1997). In contrast, no *Zic3* expression was detected in the bafilomycin A1-treated embryos (Fig. 4d).

Discussion

Transmembrane H⁺ fluxes are known to play a role in regulating the cytoplasmic pH of cells during fertilization and early animal
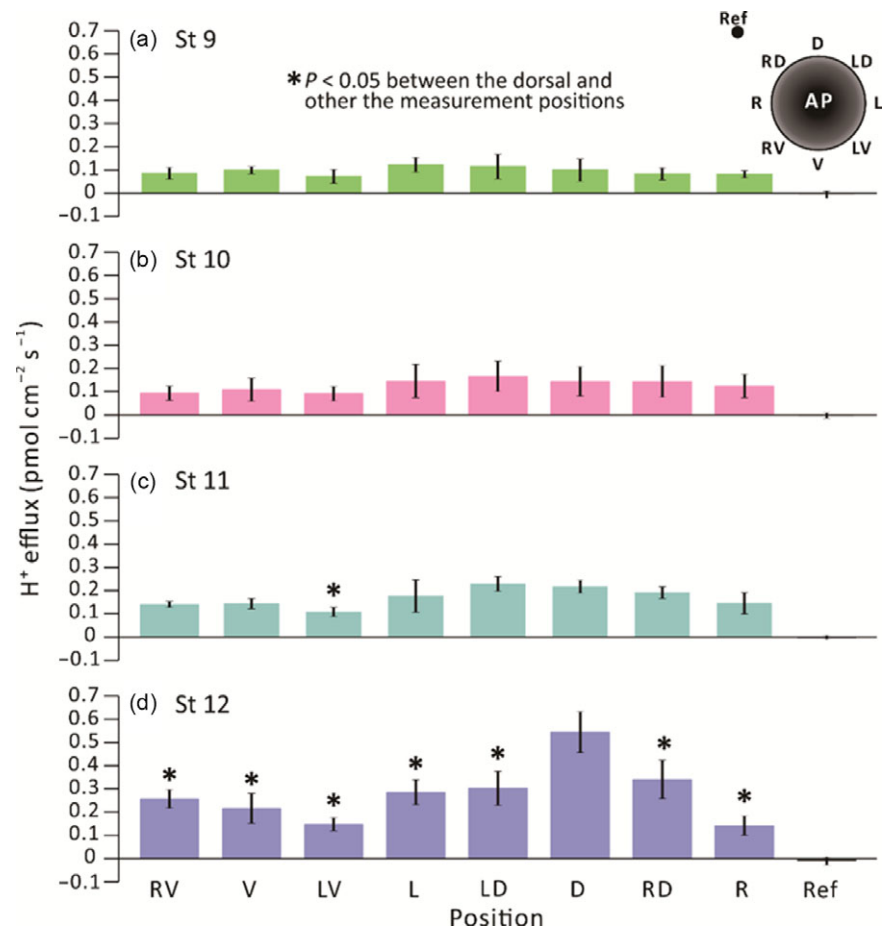
Figure 2. SIET measurements showing the H^+ fluxes recorded around the equatorial circumference of *X. laevis* embryos from stages 9 to 12 (i.e. ~7–13.25 hpf). H^+ fluxes were measured in eight positions around embryos, as shown in the schematic on the upper right corner of panel (a). Fluxes were measured at (a) stage 9; (b) stage 10; (c) stage 11; and (d) stage 12 at an elevation of ~200 μm above the embryonic equator. The data represent the mean ± standard error of the mean (SEM) of $n = 5$ embryos for each stage measured. The reference point (Ref) was measured at a distance of ~5 mm away from the embryo. In (c) and (d), the asterisks indicate that H^+ efflux data acquired around the embryo were significantly lower ($P < 0.05$) than those acquired on the dorsal side. Statistical significance was tested by two-way ANOVA and Tukey's honest significant difference test.

development (Johnson and Epel, 1976; Gillespie and Greenwell, 1988; Baltz *et al.*, 1993; Faszewski and Kunkel, 2001; Adams *et al.*, 2006; Ebanks *et al.*, 2010). Here, we applied the non-invasive extracellular SIET in an H^+-sensitive configuration and demonstrated the presence of a significantly higher H^+ efflux on the dorsal side of intact *X. laevis* embryos at stage 12 when compared with the H^+ effluxes at the other measuring positions around the embryo (Figs 2 and 3). This is the first direct, truly non-invasive measurement of such a phenomenon during the late gastrula stage of *X. laevis* development. Our new data support and confirm those described previously, in which it was reported that *X. laevis* embryos exhibit an intracellular alkalinization in the dorsal ectoderm cells during neural induction (Sater *et al.*, 1994). In this earlier report, *X. laevis* planar explants loaded with the fluorescent pH indicator BCECF-dextran, were monitored by emission ratio microfluorimetry. As the increase in pH_i was not detected in ectodermal cells in planar explants dissected from the ventral marginal zone or if the dorsal ectoderm was isolated from the inductive activity of the mesodermal cells, the authors suggested that it might be one of the factors required for determining the anterior neural fate of the ectoderm (Sater *et al.*, 1994). We suggest that this neutralizing intracellular alkalinization might, at least in part, contribute to the localized H^+ efflux across the plasma membranes of the dorsal epithelial cells that we recorded.

We considered it important to confirm and extend the original data reported by Sater *et al.* (1994). For example, some problems have been reported when using BCECF-dextran to measure pH_i due to prolonged photobleaching of the dye, which can result in erroneous measurements (Weiner and Hamm, 1989;

Han and Burgess, 2010). However, Sater *et al.* (1994) adopted protocols to minimize possible photobleaching, such as utilizing both continuous and intermittent imaging strategies, as well as incorporating neutral density filters to reduce the intensity of the required excitation light. Another factor to consider is that the early BCECF-dextran imaging experiments were conducted *ex vivo* with planar embryonic explants (Keller and Danilchik, 1988) rather than in intact embryos. The experimental protocol involved microinjecting the reporter dye into the dorsal blastomeres of 32-cell stage embryos, then planar explants were dissected from the dorsal or ventral marginal zones at the start of gastrulation. Furthermore, the external epithelium was removed from the planar explant prior to imaging to improve the optical conditions for microfluorimetry in the underlying layers. Any of these procedures, therefore, might have induced a pH_i-related artefact. Therefore, we considered it important to conduct our experiments in intact, normally developing embryos. However, despite the differences in protocol, the similarities between the BCECF-dextran data reported by Sater *et al.* (1994) and our new SIET-derived data with respect to the spatial nature of the embryonic domain generating the efflux of H^+ (and the developmental time window), suggest that the localized H^+ flux is a reproducible phenomenon associated with neural induction in *X. laevis*. In addition, this suggests that the precautions taken by Sater *et al.* (1994) to limit the deleterious effects of photobleaching (and therefore dye reliability) were largely successful. Furthermore, the ability to recapitulate a developmental event from an intact embryo in an embryonic tissue explant illustrates the robust nature of *X. laevis* embryos as a developmental model (DeSimone *et al.*, 2005). It also demonstrates that tissue explants are effective *ex vivo* models for
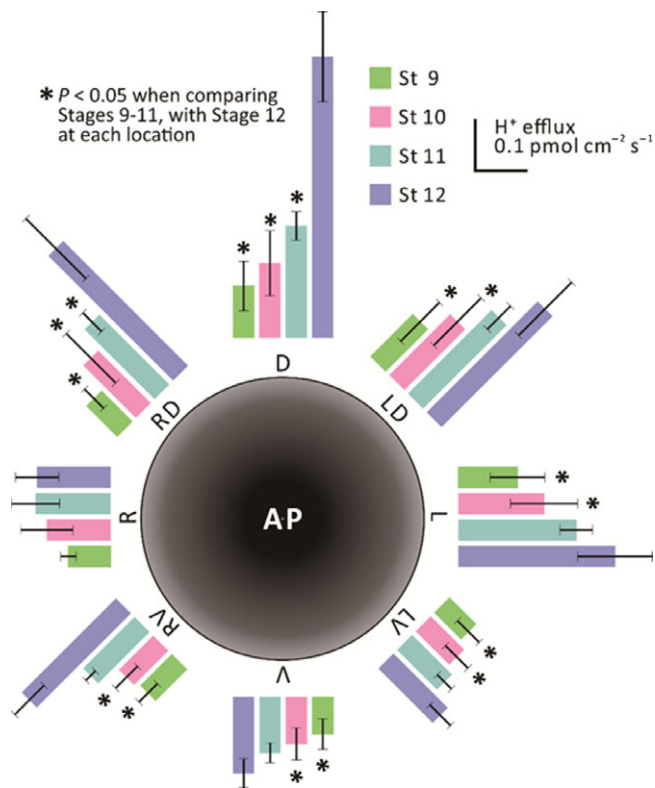
Figure 3. Comparison of H^+ flux data in different locations around the equatorial circumference of *X. laevis* embryos between stages 9 to 12 (i.e. ~7–14.25 hpf). The data shown in Fig. 2 were also plotted as a radial column chart to allow comparison between the stages for each measurement position. The results show that, at stage 12, the H^+ effluxes at all the measuring positions except the right side are significantly higher ($P < 0.05$) than those at the same side at stage 9 and stage 10. Similarly, the H^+ effluxes on the right dorsal and dorsal sides at stage 12 are significantly higher ($P < 0.05$) than that on the same side at stage 11. Statistical significance was tested by two-way analysis of variance (ANOVA) test and Tukey's honestly significant difference test.

deciphering the complex three-dimensional signalling events that take place between different tissue layers (Keller and Danilchik, 1988).

Proton pumping vacuolar-ATPases (V-ATPases) have diverse functions from acidifying the lumen of a variety of intracellular organelles (Futai *et al.*, 2019; Banerjee and Kane, 2020) to generating H^+ effluxes across the plasma membranes of different cell types (Nanda *et al.*, 1996; Wagner *et al.*, 2004; Jouhou *et al.*, 2007). As such, they play a key role in the regulation of intracellular and intercellular signalling pathways (Pamarthy *et al.*, 2018). For example, an active V-ATPase was reported to be expressed in the plasma membrane of *X. laevis* embryos as early as the 4-cell stage, where it was shown to play a key role in the left–right patterning of the embryo (Adams *et al.*, 2006). It has been suggested that the function of such a V-ATPase-dependent H^+ efflux is to hyperpolarize the plasma membrane and increase the pH of the cytoplasm (Swallow *et al.*, 1990; Adams *et al.*, 2006; Vandenberg *et al*., 2011). Considering these reports, we treated *X. laevis* embryos with the specific V-ATPase inhibitor, bafilomycin A1 (Yoshimori *et al.*, 1991), from stages 9 to 12, and therefore began to explore the possible function(s) of the late gastrula period H^+ efflux we detected. The inhibition of V-ATPase activity during this key developmental period led to a variable level of inhibition of blastopore closure and the subsequent failure to form early neural structures (Fig. 4b). Clearly, treatment with bafilomycin A1 will

inhibit all the cellular V-ATPases located in the plasma membrane as well as those of the intracellular organelles, and therefore may result in numerous secondary developmental and physiological effects. For example, they are known to attenuate two-pore channel-mediated Ca^{2+} release from lysosomes (Patel *et al.*, 2010). This might, in turn, result in various developmental defects including those that arise during neurogenesis (Guo *et al.*, 2020). A similar finding has previously been described when *X. laevis* embryos were treated with bafilomycin for 24 h starting at the 2-cell stage; this led to an inhibition of gastrulation and convergent extension movements (Coombs *et al.*, 2010). We showed that bafilomycin A1 treatment also led to the downregulation of *Zic3* expression (Fig. 4d). This suggests that V-ATPase activity and pH_i might also play an important signalling role during the gastrula period with regards to neural gene expression. It is not possible at this time to determine if bafilomycin A1 had a direct effect on the signal transduction pathway leading to the expression of *Zic3*, or if the effect was secondary; for example, resulting from a cessation of the morphogenic movements that contributed to gastrulation. However, it is becoming clear that neural induction is regulated via a complex interplay between cell-to-cell signalling, inductive interactions, morphogenetic movements, and localized gene expression (Keller *et al.*, 1992; Nakata *et al.*, 1997; Muñoz-Sanjuán *et al.*, 2002; Leclerc *et al.*, 2012; Stern, 2006; Néant *et al.*, 2019). It will, therefore, require careful and extended experimentation to decipher exactly where and when the H^+ fluxes occur (perhaps at various times and in different intracellular and/or embryonic locations) during the extended process of neural induction and subsequent neurogenesis. For example, it has been shown via the use of voltage and pH dyes, that a wave of bioelectrical activity travels across the ectoderm of intact *X. laevis* embryos during neurulation, and that inhibiting V-ATPases leads to abnormalities in craniofacial morphogenesis (Vandenberg *et al.*, 2011). Furthermore, it has been demonstrated that a V-ATPase is expressed strongly in the neural tissues and head of *X. laevis* during the later tail bud stages (Rutenberg *et al.*, 2002).

We did not investigate the effect of bafilomycin A1 on the dorsal H^+ fluxes. However, it has previously been reported that H^+ fluxes measured using a SIET similar to ours across the pseudostratified epithelium in the proximal region of the vas deferens in rat (Breton *et al.*, 2016), were drastically reduced by treatment with bafilomycin A1 (Smith and Trimarchi, 2001). Bafilomycin A1 has also been shown to reduce $[H^+]$ gradients (again measured using a similar SIET to ours), in the anterior midgut of mosquito (*Aedes* sp.) larvae (Boudko *et al.*, 2001). Moreover, in *X. laevis* embryos, concanamycin (another specific H^+-V-ATPase inhibitor; Whyteside *et al.*, 2005) was shown to reduce the efflux of H^+ (and block the formation of left–right asymmetry) during early development (Adams *et al.*, 2006). This suggests that the H^+ fluxes we recorded are likely to also be inhibited by an H^+-V-ATPase inhibitor such as bafilomycin A1 (or concanamycin).

V-ATPase activity has also been shown to be required for (and in some situations it might directly regulate) Wnt signalling (Cruciat *et al.*, 2010; Sun-Wada and Wada, 2015; Oginuma *et al.*, 2020). In addition, a Wnt signal at the cleavage stage in *X. laevis* embryos has been reported to play a role in activating subsequent neural development (Baker *et al.*, 1999). It has also been proposed that binding of the Wnt ligand to the Wnt receptor complex requires a V-ATPase-mediated H^+ efflux (Sun-Wada and Wada, 2015) and that bafilomycin A1 inhibits Wnt signalling (Cruciat *et al.*, 2010). Therefore, the precise relationship between V-ATPase activity, H^+ efflux, and Wnt signalling is still far from
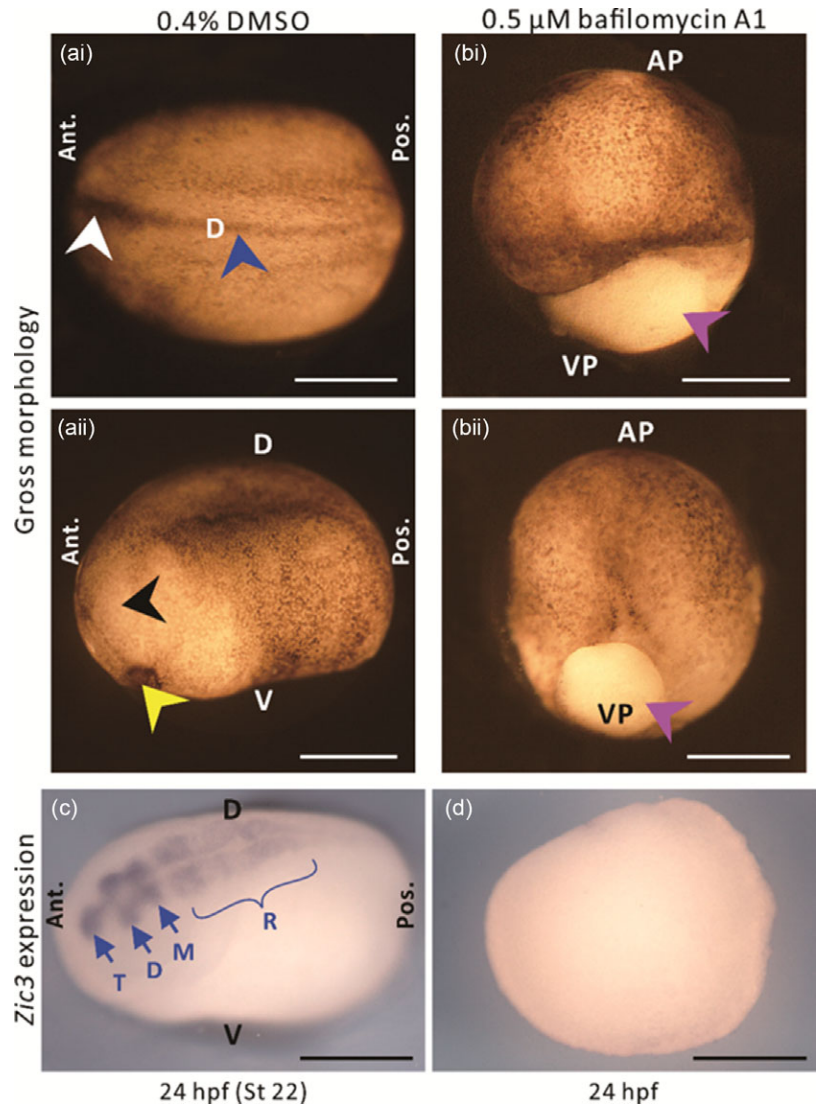
Figure 4. The effect of the V-ATPase blocker, bafilomycin A1 on the gross morphology and expression of the *Zic3* gene in embryos at the neurula stage. (a, b) Gross morphology and (c, d) *Zic3* gene expression of embryos treated with either (a, c) 0.4% DMSO or (b, d) 0.5 μM bafilomycin A1, from ~7–13.25 hpf (i.e. equivalent to stages 9–12 in untreated, normally developing embryos). Embryos were fixed at ~24 hpf (i.e. equivalent to stage 22 in untreated, normally developing embryos), and top-illuminated images were acquired either (a, b) immediately or (c, d) after *in situ* hybridization was conducted to detect *Zic3* mRNA. Panels (ai), (aii), (bi) and (bii) show different embryos. In (ai, aii), the white, blue, black, and yellow arrowheads indicate the unfused and fused neural folds, eye anlage, and cement gland, respectively, whereas in (bi, bii), the purple arrowheads indicate the yolk plug. In (c), T, D, M and R indicate the telencephalon, diencephalon, mesencephalon and rhombencephalon, respectively. AP, VP, D, V, Ant., and Pos. are animal pole, vegetal pole, dorsal, ventral, anterior, and posterior, respectively. Scale bars, 500 μm.

clear. Our new data, however, add to the growing evidence first proposed by Sater *et al.* (1994) for an increase in pH$_i$ via a V-ATPase-mediated H$^+$ efflux playing a role in regulating neural induction in *X. laevis* embryos. It has, however, also been reported in tail bud cells from chick embryos that increased pH$_i$ promotes acetylation of non-enzymatic β-catenin downstream of Wnt signalling (Oginuma *et al.*, 2020), and that acetylated β-catenin promotes mesodermal rather than neural fate (Hoffmeyer *et al.*, 2017). There is, therefore, still much to understand with regards to the relationship between pH$_i$ dynamics and Wnt signalling during the different phases of neurogenesis in different embryonic domains. In addition to accumulating evidence suggesting the function of a V-ATPase-driven H$^+$ extrusion across the plasma membrane, alternate complementary mechanisms might also play a role in the alkalinization of dorsal ectoderm cell cytoplasm during neural induction. These include Na$^+$/H$^+$ exchange and Na$^+$-dependent Cl$^-$/HCO$_3^-$ exchange. While the former has been reported during fertilization in sea urchin eggs and in preimplantation mouse embryos (Epel, 1980; Siyanov and Baltz, 2013), it does not appear to play a role in the early development of *X. laevis* embryos (Webb and Nuccitelli 1981; Sater *et al.*, 1994). For example, when dorsal marginal zone explants were treated with the protein kinase C and Na$^+$/H$^+$ exchange agonist TPA

(12-O-tetradecanoyl phorbol-13-acetate), the cells experienced an immediate decrease (rather than the expected increase) in pH$_i$ and the explants dissociated rapidly (Sater *et al.*, 1994). There is, however, evidence for a role for Na$^+$-dependent Cl$^-$/HCO$_3^-$ exchange in the alkalinization that occurs during neural induction in *X. laevis* embryos. For example, when explants at early stage 10.5 were treated with the anion transport inhibitor 4,4′-dihydrodiisothiocyanatostilbene-2,2′-disulfonate, or when the [Na$^+$] and [Cl$^-$] in the bathing solution was decreased and increased, respectively, then the normal increase in pH$_i$ and tissue-specific expression of the neural gene *engrailed-2* were both blocked (Sater *et al.*, 1994).

It is still unknown if the V-ATPase-generated H$^+$ fluxes mediate their effect via hyperpolarization of the plasma membrane or due to an alkalization of the cytoplasm of dorsal ectoderm cells, or indeed via a combination of both processes. Although it has been reported that H$^+$ pump-dependent changes in membrane voltage are an early and necessary mechanism to induce *X. laevis* tail regeneration (Adams *et al.*, 2007), we suggest that the relatively long lasting slow-changing H$^+$ fluxes we recorded are likely to be involved in the intracellular alkalinization that has been reported to be important for some early development processes in several species (Winkler *et al.*, 1980; Baltz *et al.*, 1993; Phillips *et al.*, 2000).

It has previously been reported from *X. laevis* embryos that localized, intracellular Ca^{2+} transients triggered by planar signals can induce the expression of the *Zic3* gene in the dorsal ectoderm during neural induction (Leclerc *et al.*, 2003; Batut *et al.*, 2005; Néant *et al.*, 2019). We propose that an increase in pH_i might be associated in some required/synergistic way with these Ca^{2+} transients to induce the expression of important early primary genes known to regulate the subsequent expression of other essential neural genes (Nakata *et al.*, 1997; Winata *et al.*, 2013). Such ionic and multi-step regulation of gene expression is well recognized (Vanden Broeck *et al.*, 1992; Calkhoven and Ab, 1996). Indeed, it has previously been reported that when *X. laevis* dorsal marginal zone planar explants were treated with the anion transport inhibitor 4,4′-dihydrodiisothiocyanatostilbene-2,2′-disulfonate to block the normal intracellular alkalinization, then the expression of neural-specific genes (i.e. *NCAM* and *otx2*) were either reduced or completely missing (Uzman *et al.*, 1998). In addition, when uninduced animal cap ectoderm was precociously alkalinized by treatment with methylamine or NH_4Cl, then *NCAM*, *otx2* and *noggin* (an anterior neural inducer gene) were all expressed. Furthermore, alkalinization of the ectoderm at stage 10.5 elicited a rapid increase (i.e. within ~15 min) in the expression of *otx2* (Uzman *et al.*, 1998).

It is also known that gap junction conductance is sensitive to pH_i (Spray *et al.*, 1981; Peracchia, 2004) and it has been suggested that localized Ca^{2+} transients generated in the anterior dorsal ectoderm, which that are required for neural induction, might pass from cell to cell through gap junctions (Leclerc *et al.*, 2000, 2012; Belousov and Fontes, 2013). We suggest that this might, therefore, provide a link between Ca^{2+} and H^+ being involved in the synergistic regulation of *Zic3* expression and subsequent neural induction in the dorsal ectoderm of *X. laevis* embryos. This adds another layer of complexity to the interaction between the multiple ectodermal and endomesodermal signals (including Chordin, Noggin, BMP4, Wnts, β-catenin, Cerberus, various Ca^{2+} channels and H^+) and gene expression, which combine to regulate the complex process of neural induction in *X. laevis* (Sater *et al.*, 1994; Baker *et al.*, 1999; Kuroda *et al.*, 2004; Stern, 2006; Moreau *et al.*, 2008, 2009, 2020; Cho *et al.*, 2014; Néant *et al.*, 2019). Our new data therefore add to the accumulating evidence that suggests that intracellular alkalinization might contribute to establishing anterior neural fate in *X. laevis* embryos.

Conflict of interest. The authors declare none.

Ethical approval. All the procedures used in this study were performed in accordance with the guidelines and regulations set out by the Animal Ethics Committee of the HKUST and by the Department of Health, Hong Kong.

References

Adams DS, Robinson KR, Fukumoto T, Yuan S, Albertson RC, Yelick P, Kuo L, McSweeney M and Levin M (2006). Early, H^+-V-ATPase-dependent proton flux is necessary for consistent left–right patterning of non-mammalian vertebrates. *Development* **133**, 1657–71.

Adams DS, Masi A and Levin M (2007). H^+ pump-dependent changes in membrane voltage are an early mechanism necessary and sufficient to induce *Xenopus* tail regeneration. *Development* **134**, 1323–35.

Adlimoghaddam A, Weihrauch D and O'Donnell MJ (2014). Localization of K^+, H^+, Na^+ and Ca^{2+} fluxes to the excretory pore in *Caenorhabditis elegans*: application of scanning ion-selective microelectrodes. *J Exp Biol* **217**, 4119–22.

Altizer AM, Moriarty LJ, Bell SM, Schreiner CM, Scott WJ and Borgens RB (2001). Endogenous electric current is associated with normal development of the vertebrate limb. *Dev Dynam* **221**, 391–401.

Baker JC, Beddington RSP and Harland RM (1999). Wnt signaling in *Xenopus* embryos inhibits *Bmp4* expression and activates neural development. *Genes Dev* **13**, 3149–3159.

Baltz JM, Biggers JD and Lechene C (1993). A novel H^+ permeability dominating intracellular pH in the early mouse embryo. *Development* **118**, 1353–61.

Banerjee S and Kane PM (2020). Regulation of V-ATPase activity and organelle pH by phosphatidylinositol phosphate lipids. *Front Cell Dev Biol* **8**, 510.

Batut J, Vandel L, Leclerc C, Daguzan C, Moreau M and Néant I (2005). The Ca^{2+}-induced methyltransferase xPRMT1b controls neural fate in amphibian embryo. *Proc Natl Acad Sci USA* **102**, 15128–33.

Beane WS, Morokuma J, Lemire JM and Levin M (2013). Bioelectric signaling regulates head and organ size during planarian regeneration. *Development* **140**, 313–22.

Belousov AB and Fontes JD (2013). Neuronal gap junctions: Making and breaking connections during development and injury. *Trends Neurosci* **36**, 227–36.

Borgens RB, Vanable Jr, JW and Jaffe LF (1977). Bioelectricity and regeneration: Large currents leave the stumps of regenerating newt limbs. *Proc Natl Acad Sci USA* **74**, 4528–32.

Boudko DY, Moroz LL, Linser PJ, Trimarchi JR, Smith PJS and Harvey WR (2001). *In situ* analysis of pH gradients in mosquito larvae using non-invasive, self-referencing, pH-sensitive microelectrodes. *J Exp Biol* **204**, 691–9.

Bowman EJ, Siebers A and Altendorf K (1988). Bafilomycins: A class of inhibitors of membrane ATPases from microorganisms, animal cells, and plant cells. *Proc Natl Acad Sci USA* **85**, 7972–6.

Breton S, Ruan YC, Park YJ and Kim B (2016). Regulation of epithelial function, differentiation, and remodeling in the epididymis. *Asian J Androl* **18**, 3–9.

Calkhoven CF and Ab G (1996). Multiple steps in the regulation of transcription-factor level and activity. *Biochem J* **317**, 329–42.

Cao L, Wei D, Reid B, Zhao S, Pu J, Pan T, Yamoah E and Zhao M (2013). Endogenous electric currents might guide rostral migration of neuroblasts. *EMBO Rep* **14**, 184–90.

Carraretto L, Teardo E, Checchetto V, Finazzi G, Uozumi N and Szabo I (2016). Ion channels in plant bioenergetic organelles, chloroplasts and mitochondria: From molecular identification to function. *Molecular Plant*, **9**, 371–95.

Carvacho I, Piesche M, Maier TJ and Machaca K (2018). Ion channel function during oocyte maturation and fertilization. *Front Cell Dev Biol* **6**, 63.

Chan CM, Chen Y, Hung TS, Miller AL, Shipley AM and Webb SE (2015). Inhibition of SOCE disrupts cytokinesis in zebrafish embryos via inhibition of cleavage furrow deepening. *Int J Dev Biol* **59**(7–9), 289–301.

Cho A, Tang Y, Davila J, Deng S, Chen L, Miller E, Wernig M and Graef IA (2014). Calcineurin signaling regulates neural induction through antagonizing the BMP pathway. *Neuron* **82**, 109–24.

Coombs GS, Yu J, Canning CA, Veltri CA, Covey TM, Cheong JK, Utomo V, Banerjee N, Zhang ZH, Jadulco RC, Concepcion GP, Bugni TS, Harper MK, Mihalek I, Jones CM, Ireland CM and Virshup DM (2010). WLS-dependent secretion of WNT3A requires Ser209 acylation and vacuolar acidification. *J Cell Sci* **123**, 3357–67.

Cruciat CM, Ohkawara B, Acebron SP, Karaulanov E, Reinhard C, Ingelfinger D, Boutros M and Niehrs C (2010). Requirement of prorenin receptor and vacuolar H^+-ATPase–mediated acidification for Wnt signaling. *Science* **327**(5964), 459–63.

Dedic C, Hung TS, Shipley AM, Maeda A, Gardella T, Miller AL, Divieti Pajevic P, Kunkel JG and Rubinacci A (2018). Calcium fluxes at the bone/plasma interface: Acute effects of parathyroid hormone (PTH) and targeted deletion of PTH/PTH-related peptide (PTHrP) receptor in the osteocytes. *Bone* **116**, 135–43.

DeSimone DW, Davidson L, Marsden M and Alfandari D (2005). The *Xenopus* embryo as a model system for studies of cell migration. In J. L. Guan (Ed.), *Cell Migration. Methods in Molecular Biology*, 294. Humana Press.

De Simone ML, Grumetto L, Tosti E, Wilding M and Dale B (1998). Non-specific currents at fertilisation in sea urchin oocytes. *Zygote* **6**, 11–5.

Doniach T, Phillips CR and Gerhart JC (1992). Planar induction of anteroposterior pattern in the developing central nervous system of *Xenopus laevis*. *Science* **257**(5069), 542–5.

Duthie GG, Shipley A and Smith PJS (1994). Use of a vibrating electrode to measure changes in calcium fluxes across the cell membranes of oxidatively challenged *Aplysia* nerve cells. *Free Radic Res* **20**, 307–13.

Ebanks SC, O'Donnell MJ and Grosell M (2010). Characterization of mechanisms for Ca^{2+} and HCO_3^-/CO_3^{2-} acquisition for shell formation in embryos of the freshwater common pond snail *Lymnaea stagnalis*. *J Exp Biol* **213**, 4092–8.

Epel D (1980). Ionic triggers in the fertilization of sea urchin eggs. *Annal NY Acad Sci* **339**, 74–85.

Faszewski EE and Kunkel JG (2001). Covariance of ion flux measurements allows new interpretation of *Xenopus laevis* oocyte physiology. *J Exp Zool* **290**, 652–61.

Feijó JA, Sainhas J, Hackett GR, Kunkel JG and Hepler PK (1999). Growing pollen tubes possess a constitutive alkaline band in the clear zone and a growth-dependent acidic tip. *J Cell Biol* **144**, 483–96.

Felle HH and Hepler PK (1997). The cytosolic Ca^{2+} concentration gradient of *Sinapis alba* root hairs as revealed by Ca^{2+}-selective microelectrode tests and fura-dextran ratio imaging. *Plant Physiol* **114**, 39–45.

Futai M, Sun-Wada GH, Wada Y, Matsumoto N and Nakanishi-Matsui M (2019). Vacuolar-type ATPase: A proton pump to lysosomal trafficking. *Proc Jpn Acad Ser B Phys Biol Sci* **95**, 261–77.

Gillespie JI and Greenwell JR (1988). Changes in intracellular pH and pH regulating mechanisms in somitic cells of the early chick embryo: A study using fluorescent pH-sensitive dye. *J Physiol* **405**, 385–95.

Guh YJ, Yang CY, Liu ST, Huang CJ and Hwang PP (2016). Oestrogen-related receptor α is required for transepithelial H^+ secretion in zebrafish. *Proc. R. Soc. B: Biol. Sci* **283**(1825), 20152582.

Guo C, Webb SE, Chan CM and Miller AL (2020). TPC2-mediated Ca^{2+} signaling is required for axon extension in caudal primary motor neurons in zebrafish embryos. *J Cell Sci* **133**, jcs244780.

Gusovsky F and Daly JW (1988). Formation of second messengers in response to activation of ion channels in excitable cells. *Cell Mol Neurobiol* **8**, 157–69.

Han J and Burgess K (2010). Fluorescent indicators for intracellular pH. *Chem Rev* **110**, 2709–28.

Harland R (2000). Neural induction. *Curr Opin Genet Dev* **10**, 357–62.

Harvey WR (1992). Physiology of V-ATPases. *J Exp Biol* **172**, 1–17.

Hemmati-Brivanlou A, Frank D, Bolce ME, Brown BD, Sive HL and Harland RM (1990). Localization of specific mRNAs in *Xenopus* embryos by whole-mount *in situ* hybridization. *Development* **110**, 325–30.

Hoffmeyer K, Junghans D, Kanzler B and Kemler R (2017). Trimethylation and acetylation of β-catenin at lysine 49 represent key elements in ESC pluripotency. *Cell Rep* **18**, 2815–24.

Hung JT, Webb SE, Palumbo C, Lesniak AM, Shipley AM, Rubinacci A, Kunkel JG and Miller AL (2019). Assessing the ability of zebrafish scales to contribute to the short-term homeostatic regulation of $[Ca^{2+}]$ in the extracellular fluid during calcemic challenges. *Fish Sci* **85**, 943–59.

Hunter GL, Crawford JM, Genkins JZ and Kiehart DP (2014). Ion channels contribute to the regulation of cell sheet forces during *Drosophila* dorsal closure. *Development* **141**, 325–334.

Jaffe LF (1979). Control of development by ionic currents. In R. A. Cone & J. E. Dowling (Eds.), *Membrane Transduction Mechanisms* (pp. 199–231). Raven Press.

Jaffe LF (1981). The role of ionic currents in establishing developmental pattern. *Phil Trans R Soc Lond Ser B, Biol Sci* **295**(1078), 553–66.

Jaffe LF and Nuccitelli R (1974). An ultrasensitive vibrating probe for measuring steady extracellular currents. *J Cell Biol* **63**(2 Pt 1), 614–28.

Jaffe LF and Stern CD (1979). Strong electrical currents leave the primitive streak of chick embryos. *Science* **206**(4418), 569–571.

Jamieson L, Waters A, Ho KE, Chan HYS, Hung JT, Webb SE, Chan CM, Shipley AM, Williamson JG, Beer J, Angus C and Miller AL (2021). Short-term homeostatic regulation of blood/interstitial fluid Ca^{2+} concentration by the scales of anadromous sea trout *Salmo trutta* L. during smoltification and migration. *J Fish Biol* **98**, 17–32.

Johnson JD and Epel D (1976). Intracellular pH and activation of sea urchin eggs after fertilisation. *Nature* **262**(5570), 661–4.

Jones DL, Shaff JE and Kochian LV (1995). Role of calcium and other ions in directing root hair tip growth in *Limnobium stoloniferum*: I. Inhibition of tip growth by aluminum. *Planta* **197**, 672–80.

Jouhou H, Yamamoto K, Homma A, Hara M, Kaneko A and Yamada M (2007). Depolarization of isolated horizontal cells of fish acidifies their immediate surrounding by activating V-ATPase. *J Physiol* **585**, 401–12.

Kay BK and Peng HB (1991). *Xenopus laevis: Practical Uses in Cell and Molecular Biology*, **36**. Academic Press.

Keller RE (1984). The cellular basis of gastrulation in *Xenopus laevis*: Active, postinvolution convergence and extension by mediolateral interdigitation. *Am Zool* **24**, 589–603.

Keller R and Danilchik M (1988). Regional expression, pattern and timing of convergence and extension during gastrulation of *Xenopus laevis*. *Development* **103**, 193–209.

Keller R, Shih J, Sater AK and Moreno C (1992). Planar induction of convergence and extension of the neural plate by the organizer of *Xenopus*. *Dev Dynam* **193**, 218–34.

Kline D, Robinson KR and Nuccitelli R (1983). Ion currents and membrane domains in the cleaving *Xenopus* egg. *J Cell Biol* **97**, 1753–61.

Kochian LV, Shaff JE, Kühtreiber WM, Jaffe LF and Lucas WJ (1992). Use of an extracellular, ion-selective, vibrating microelectrode system for the quantification of K^+, H^+, and Ca^{2+} fluxes in maize roots and maize suspension cells. *Planta* **188**, 601–10.

Kropf DL, Caldwell JH, Gow NAR and Harold FM (1984). Transcellular ion currents in the water mold *Achlya*. Amino acid proton symport as a mechanism of current entry. *J Cell Biol* **99**, 486–96.

Kühtreiber WM and Jaffe LF (1990). Detection of extracellular calcium gradients with a calcium-specific vibrating electrode. *J Cell Biol* **110**, 1565–73.

Kuroda H, Wessely O and De Robertis EM (2004). Neural induction in *Xenopus*: Requirement for ectodermal and endomesodermal signals via chordin, noggin, β-catenin, and Cerberus. *PLoS Biol* **2**, E92.

Lamb TM and Harland RM (1995). Fibroblast growth factor is a direct neural inducer, which combined with noggin generates anterior–posterior neural pattern. *Development* **121**, 3627–36.

Leclerc C, Webb SE, Daguzan C, Moreau M and Miller AL (2000). Imaging patterns of calcium transients during neural induction in *Xenopus laevis* embryos. *J Cell Sci* **113**, 3519–29.

Leclerc C, Lee M, Webb SE, Moreau M and Miller AL (2003). Calcium transients triggered by planar signals induce the expression of *ZIC3* gene during neural induction in *Xenopus*. *Dev Biol* **261**, 381–90.

Leclerc C, Néant I and Moreau M (2012). The calcium: An early signal that initiates the formation of the nervous system during embryogenesis. *Front Mol Neurosci* **5**, 3.

Longden TA, Hill-Eubanks DC and Nelson MT (2016). Ion channel networks in the control of cerebral blood flow. *J Cereb Blood Flow Metab* **36**, 492–512.

Luxardi G, Reid B, Ferreira F, Maillard P and Zhao M (2015). Measurement of extracellular ion fluxes using the ion-selective self-referencing microelectrode technique. *J Vis Exp* **99**, e52782.

Marenzana M, Shipley AM, Squitiero P, Kunkel JG and Rubinacci A (2005). Bone as an ion exchange organ: Evidence for instantaneous cell-dependent calcium efflux from bone not due to resorption. *Bone* **37**, 545–54.

McGillviray AM and Gow NAR (1987). The transhyphal electrical current of *Neurospora crassa* is carried principally by protons. *J Gen Microbiol* **133**, 2875–81.

McLaughlin KA and Levin M (2018). Bioelectric signaling in regeneration: Mechanisms of ionic controls of growth and form. *Dev Biol* **433**, 177–89.

Meissner G (1983). Monovalent ion and calcium ion fluxes in sarcoplasmic reticulum. *Mol Cell Biochem* **55**, 65–82.

Messerli MA, Danuser G and Robinson KR (1999). Pulsatile influxes of H^+, K^+ and Ca^{2+} lag growth pulses of *Lilium longiflorum* pollen tubes. *J Cell Sci* **112**, 1497–509.

Miller AL and Gow NAR (1989). Correlation between profile of ion-current circulation and root development. *Physiol Plant* **75**, 102–8.

Miller AL, Raven JA, Sprent JI and Weisenseel MH (1986). Endogenous ion currents traverse growing roots and root hairs of *Trifolium repens*. *Plant Cell Environ* **9**, 79–83.

Miller AL, Shand E and Gow NAR (1988). Ion currents associated with root tips, emerging laterals and induced wound sites in *Nicotians tabacum*: spatial relationship proposed between resulting electrical fields and phytophthoran zoospore infection. *Plant Cell Environ* **11**, 21–5.

Monteiro J, Aires R, Becker JD, Jacinto A, Certal AC and Rodríguez-León J (2014). V-ATPase proton pumping activity is required for adult zebrafish appendage regeneration. *PLoS One* **9**, e92594.

Moreau M, Vilain JP and Guerrier P (1980). Free calcium changes associated with hormone action in amphibian oocytes. *Dev Biol* **78**, 201–14.

Moreau M, Néant I, Webb SE, Miller AL and Leclerc C (2008). Calcium signalling during neural induction in *Xenopus laevis* embryos. *Phil Trans R Soc B* **363**(1495), 1371–5.

Moreau M, Webb SE, Néant I, Miller AL and Leclerc C (2009). Calcium signaling and cell fate determination during neural induction in amphibian embryos. In Lajtha A., Mikoshiba K. (eds) *Handbook of Neurochemistry and Molecular Neurobiology*. Springer, Boston, MA

Moreau M, Leclerc C and Néant I (2020). The saga of neural induction: Almost a century of research. *Med Sci* **36**, 1018–26.

Muñoz-Sanjuán I, Bell E, Altmann CR, Vonica A and Brivanlou AH (2002). Gene profiling during neural induction in *Xenopus laevis*: Regulation of BMP signaling by post-transcriptional mechanisms and TAB3, a novel TAK1-binding protein. *Development* **129**, 5529–40.

Nakata K, Nagai T, Aruga J and Mikoshiba K (1997). *Xenopus Zic*3, a primary regulator both in neural and neural crest development. *Proc Natl Acad Sci USA* **94**, 11980–5.

Nanda A, Brumell JH, Nordström T, Kjeldsen L, Sengeløv H, Borregaard N, Rotstein OD and Grinstein S (1996). Activation of proton pumping in human neutrophils occurs by exocytosis of vesicles bearing vacuolar-type H^+-ATPases. *J Biol Chem* **271**, 15963–70.

Néant I, Leung HC, Webb SE, Miller AL, Moreau M and Leclerc C (2019). Trpc1 as the missing link between the Bmp and Ca^{2+} signalling pathways during neural specification in amphibians. *Sci Rep* **9**, 16049.

Nieuwkoop PD and Faber J (1967). *Normal Table of Xenopus laevis (Daudin): A Systematical and Chronological Survey of the Development from the Fertilized Egg Till the End of Metamorphosis*. North-Holland Publishing Company.

Nuccitelli R (1987). The wave of activation current in the egg of the medaka fish. *Dev Biol* **122**, 522–34.

Oginuma M, Harima Y, Tarazona OA, Diaz-Cuadros M, Michaut A, Ishitani T, Xiong F and Pourquié O (2020). Intracellular pH controls WNT downstream of glycolysis in amniote embryos. *Nature* **584**(7819), 98–101.

Overall R and Jaffe LF (1985). Patterns of ionic current through *Drosophila* follicles and eggs. *Dev Biol* **108**, 102–19.

Pamarthy S, Kulshrestha A, Katara GK and Beaman KD (2018). The curious case of vacuolar ATPase: Regulation of signaling pathways. *Mol Cancer* **17**, 41.

Patel S, Marchant JS and Brailoiu E (2010). Two-pore channels: Regulation by NAADP and customized roles in triggering calcium signals. *Cell Calcium* **47**, 480–90.

Peracchia C (2004). Chemical gating of gap junction channels; roles of calcium, pH and calmodulin. *Biochim Biophys Acta* **1662**(1–2), 61–80.

Phillips KP, Léveillé MC, Claman P and Baltz JM (2000). Intracellular pH regulation in human preimplantation embryos. *Hum Reprod* **15**, 896–904.

Rathore KS, Hodges TK and Robinson KR (1988). Ionic basis of currents in somatic embryos of *Daucus carota*. *Planta* **175**, 280–9.

Reid B, Nuccitelli R and Zhao M (2007). Non-invasive measurement of bioelectric currents with a vibrating probe. *Nat Protoc* **2**, 661–9.

Robinson KR and Jaffe LF (1975). Polarizing fucoid eggs drive a calcium current through themselves. *Science* **187**(4171), 70–2.

Rutenberg J, Cheng SM and Levin M (2002). Early embryonic expression of ion channels and pumps in chick and *Xenopus* development. *Dev Dynam* **225**, 469–84.

Sater AK, Alderton JM and Steinhardt RA (1994). An increase in intracellular pH during neural induction in *Xenopus*. *Development* **120**, 433–42.

Siyanov V and Baltz JM (2013). NHE1 is the sodium–hydrogen exchanger active in acute intracellular pH regulation in preimplantation mouse embryos. *Biol Reprod* **88**, 157.

Slack C and Warner AE (1973). Intracellular and intercellular potentials in the early amphibian embryo. *J Physiol* **232**, 313–30.

Smith PJ (1995). Non-invasive ion probes—Tools for measuring transmembrane ion flux. *Nature* **378**(6557), 645–6.

Smith PJS and Trimarchi J (2001). Noninvasive measurement of hydrogen and potassium ion flux from single cells and epithelial structures. *Am J Physiol Cell Physiol* **280**, C1–11.

Spray DC, Harris AL and Bennett MVL (1981). Gap junctional conductance is a simple and sensitive function of intracellular pH. *Science* **211**(4483), 712–5.

Stern CD (2006). Neural induction: 10 years on since the "default model". *Curr Opin Cell Biol* **18**, 692–7.

Sun Z, Yue J and Zhang Q (2015). Ionic components of wound current at mouse skin incisional wounds. *Eur J BioMed Res* **1**, 3–7.

Sun-Wada GH and Wada Y (2015). Role of vacuolar-type proton ATPase in signal transduction. *Biochim Biophys Acta* **1847**, 1166–72.

Swallow CJ, Grinstein S and Rotstein OD (1990). A vacuolar type H^+-ATPase regulates cytoplasmic pH in murine macrophages. *J Biol Chem* **265**, 7645–54.

Szabo I and Zoratti M (2014). Mitochondrial channels: Ion fluxes and more. *Phys Rev* **94**, 519–608.

Talevi R and Dale B (1986). Electrical characteristics of ascidian egg fragments. *Exp Cell Res* **162**, 539–43.

Thomas RC (1972). Intracellular sodium activity and the sodium pump in snail neurones. *J Physiol* **220**, 55–71.

Thomas RC (1974). Intracellular pH of snail neurones measured with a new pH-sensitive glass micro-electrode. *J Physiol* **238**, 159–80.

Tosti E (2010). Dynamic roles of ion currents in early development. *Mol Reprod Dev* **77**, 856–67.

Tosti E, Gallo A and Silvestre F (2011). Ion currents involved in oocyte maturation, fertilization and early developmental stages of the ascidian *Ciona intestinalis*. *Mol Reprod Dev* **78**(10–11), 854–60.

Tosti E, Boni R and Gallo A (2016). Ion currents in embryo development. *Birth Defects Res. C Embryo Today* **108**, 6–18.

Tseng AS and Levin M (2008). Tail regeneration in *Xenopus laevis* as a model for understanding tissue repair. *J Dental Res* **87**, 806–16.

Uzman JA, Patil S, Uzgare AR and Sater AK (1998). The role of intracellular alkalinization in the establishment of anterior neural fate in *Xenopus*. *Dev Biol* **193**, 10–20.

Vanden Broeck J, De Loof A and Callaerts P (1992). Electrical-ionic control of gene expression. *Int J Biochem* **24**, 1907–16.

Vandenberg LN, Morrie RD and Adams DS (2011). V-ATPase-dependent ectodermal voltage and pH regionalization are required for craniofacial morphogenesis. *Dev Dynam* **240**, 1889–904.

Wagner CA, Finberg KE, Breton S, Marshansky V, Brown D and Geibel JP (2004). Renal vacuolar H^+-ATPase. *Phys Rev* **84**, 1263–314.

Webb DJ and Nuccitelli R (1981). Direct measurement of intracellular pH changes in *Xenopus* eggs at fertilization and cleavage. *J Cell Biol* **91**(2 Pt 1), 562–7.

Weiner ID and Hamm LL (1989). Use of fluorescent dye BCECF to measure intracellular pH in cortical collecting tubule. *Am J Physiol* **256**(5 Pt 2), F957–64.

Weinstein DC and Hemmati-Brivanlou A (1999). Neural induction. *Ann Rev Cell Dev Biol* **15**, 411–33.

Weisenseel MH and Jaffe LF (1976). The major growth current through lily pollen tubes enters as K$^+$ and leaves as H$^+$. *Planta* **133**, 1–7.

Weisenseel MH, Dorn A and Jaffe LF (1979). Natural H$^+$ currents traverse growing roots and root hairs of barley (*Hordeum vulgare* L.). *Plant Physiol* **64**, 512–8.

Whyteside G, Meek PJ, Ball SK, Dixon N, Finbow ME, Kee TP, Findlay JBC and Harrison MA (2005). Concanamycin and indolyl pentadieneamide inhibitors of the vacuolar H$^+$-ATPase bind with high affinity to the purified proteolipid subunit of the membrane domain. *Biochemistry* **44**, 15024–31.

Winata CL, Kondrychyn I, Kumar V, Srinivasan KG, Orlov Y, Ravishankar A, Prabhakar S, Stanton LW, Korzh V and Mathavan S (2013). Genome wide analysis reveals Zic3 interaction with distal regulatory elements of stage specific developmental genes in zebrafish. *PLOS Genet* **9**, e1003852.

Winkler MM, Steinhardt RA, Grainger JL and Minning L (1980). Dual ionic controls for the activation of protein synthesis at fertilization. *Nature* **287**(5782), 558–60.

Xu Y, Sun T and Yin L-P (2006). Application of non-invasive microsensing system to simultaneously measure both H$^+$ and O$_2$ fluxes around the pollen tube. *J Integr Plant Biol* **48**, 823–31.

Xu H, Martinoia E and Szabo I (2015). Organellar channels and transporters. *Cell Calcium* **58**, 1–10.

Yoshimori T, Yamamoto A, Moriyama Y, Futai M and Tashiro Y (1991). Bafilomycin A1, a specific inhibitor of vacuolar-type H$^+$-ATPase, inhibits acidification and protein degradation in lysosomes of cultured cells. *J Biol Chem* **266**, 17707–12.

Zhu MX, Ma J, Parrington J, Galione A and Evans AM (2010). TPCs: endolysosomal channels for Ca^{2+} mobilization from acidic organelles triggered by NAADP. *FEBS Lett* **584**, 1966–74.

Zonia L, Cordeiro S, Tupý J and Feijó JA (2002). Oscillatory chloride efflux at the pollen tube apex has a role in growth and cell volume regulation and is targeted by inositol 3,4,5,6-tetra*kis*phosphate. *Plant Cell* **14**, 2233–49.

Živanović BD (2012). Surface tip-to-base Ca^{2+} and H$^+$ ionic fluxes are involved in apical growth and graviperception of the *Phycomyces* stage I sporangiophore. *Planta* **236**, 1817–29.